Iron Oxide @ Polypyrrole Nanoparticles as a Multifunctional Drug Carrier for Remotely Controlled Cancer Therapy with Synergistic Antitumor Effect

Chao Wang,[†,§] Huan Xu,[†,§] Chao Liang,[†] Yumeng Liu,[‡] Zhiwei Li,[†] Guangbao Yang,[†] Liang Cheng,[†] Yonggang Li,[‡] and Zhuang Liu[†,*]

[†]Jiangsu Key Laboratory for Carbon-Based Functional Materials & Devices, Institute of Functional Nano & Soft Materials (FUNSOM), Soochow University, Suzhou, Jiangsu 215123, China and [‡]Department of Radiology, The First Affiliated Hospital of Soochow University, Suzhou, Jiangsu 215006, China. [§]C. Wang and H. Xu contributed equally.

ABSTRACT Multifunctional nanoplatforms that are safe and have multiple therapeutic functions together with imaging capabilities are highly demanded in the development of new cancer theranostic approaches. A number of near-infrared (NIR)-absorbing inorganic nanomaterials, although having shown great promise not only to photothermally ablate tumors but also to enhance the efficacy of other types of therapies, are not biodegradable and would be retained in the body for a long time. Herein, we develop a multifunctional nanocomposite by coating magnetic iron oxide nanoclusters with a near-infrared light-absorbing polymer polypyrrole (PPy), obtaining Fe_3O_4@PPy core–shell nanoparticles, which after functionalization with polyethylene glycol could be used for imaging-guided, remotely controlled cancer combination therapy. In this system, the Fe_3O_4 core, which could be gradually decomposed in physiological environments, is useful for magnetically controlled drug delivery as well as a magnetic resonance imaging contrast. The PPy shell, as an organic polymer, is able to load therapeutic molecules with aromatic structures and also exhibits a strong photothermal effect, which can be used to enhance the chemotherapeutic efficacy, showing an outstanding *in vivo* synergistic antitumor effect. Our work encourages further exploration of light-absorbing polymer-based nanocomposites for cancer combination therapy under remote physical controls.

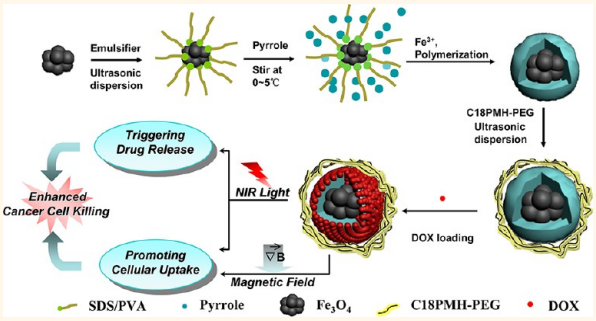

KEYWORDS: polypyrrole · iron oxide nanoclusters · drug delivery · photothermal · magnetic · cancer combination therapy

The development of external stimulus-responsive nanoparticle systems for remotely controllable cancer therapies has received significant attention in recent years, as these systems can differentially increase drug accumulation at targeted lesions, drastically decrease systemic toxicity, and potentially avoid under- or overdosing.[1,2] A variety of external physical stimuli, including light, magnetic field, electric field, heat, and ultrasound, have been utilized to trigger, control, and/or enhance localized cancer therapies.[3−9] Among different external stimuli, near-infrared (NIR) light (650−900 nm) has become an attractive one because of its easy operation, the ability to be locally focused on a specific region, and its minimal absorbance by skin and tissues to allow for noninvasive penetration of reasonably deep tissues. Employing different types of light-absorbing agents, NIR light can be effectively converted into heat as the result of a photothermal effect to "cook" cancer cells.[10−12] Besides using heat to directly destroy cancer, the photothermal effect can be taken advantage of to stimulate other types of therapies by enabling NIR-responsive on-demand release or delivery of therapeutics for combined cancer treatment, which offers a synergistically enhanced therapeutic efficacy compared with monotherapy.[13,14]

A variety of nanomaterials, most of them inorganic ones including gold nanomaterials (Au nanoshells,[15] nanorods,[16] and nanocages[17,18]), carbon nanomaterials (carbon nanotube[12] and graphene[11,19]), palladium nanosheets,[20] and copper sulfide nanoparticles,[21] have been widely studied

* Address correspondence to zliu@suda.edu.cn.

Received for review April 8, 2013 and accepted July 3, 2013.

Published online July 03, 2013
10.1021/nn4017179

as photothermal therapy (PTT) nanoagents in the past decade. However, those inorganic nanomaterials are nonbiodegradable and usually would remain in the body for long periods of time, raising concerns regarding their potential long-term toxicity. Therefore, nontoxic and more biocompatible PTT agents, such as organic ones, urgently need to be developed. Very recently, light-absorbing organic polymeric nanoparticles have acquired wide attention as PTT agents.[22−25] Among several different NIR light-absorbing polymers, polypyrrole (PPy), which is widely used as a biomaterial in biosensing and tissue engineering (*e.g.*, nerve regeneration),[24,26−30] has been demonstrated to exhibit good biocompatibility in a number of previous studies *in vitro* and *in vivo*.[31−35] Furthermore, with strong NIR absorbance, PPy nanoparticles have also been explored by several groups including ours as a new PTT agent for photothermal treatment of cancer *in vitro* and *in vivo*.[24,36,37] Further efforts, however, are still demanded to develop PPy-based theranostic nanoagents for remotely controllable cancer combination therapy.

In this work, we fabricate a NIR-response multifunctional drug delivery platform based on PPy-coated magnetic nanoparticles for combined cancer therapy under remote physical control. Iron oxide, chosen in our study as a superparamagnetic iron oxide (SPIO) nanoparticle agent, is one of the very few types of inorganic-based nanomaterials approved for clinical use and shows great biocompatibility. Clusters of ultrasmall iron oxide magnetic nanoparticles are coated with the NIR light-absorbing PPy polymer by *in situ* polymerization, obtaining Fe_3O_4@PPy core−shell nanoparticles, which are then modified with polyethylene glycol (PEG) to acquire water solubility. An aromatic chemotherapy drug, doxorubicin (DOX), can be effectively loaded into the PPy shell of those Fe_3O_4@PPy-PEG nanoparticles, likely *via* hydrophobic interaction and $\pi-\pi$ stacking. Using DOX-loaded nanoparticles as the model system, it is uncovered that the intracellular uptake of Fe_3O_4@PPy-PEG-DOX could be stimulated not only by an external magnetic field but also by NIR laser irradiation due to mild photothermal heating. On the other hand, after cell internalization, the release of DOX from Fe_3O_4@PPy-PEG-DOX localized inside cell endosomes or lysosomes could also be triggered by NIR laser exposure. The combined therapy is then demonstrated in both *in vitro* cell culture and *in vivo* animal experiments, achieving excellent synergistic therapeutic efficacy. The magnetic core of those nanoparticles could further be utilized as the T2 contrast agent in magnetic resonance (MR) imaging to track tumor development after treatment. Our results not only promise the use of Fe_3O_4@PPy core−shell nanoparticles for imaging-guided combined cancer therapies but also encourage further exploration of other light-absorbing polymers and their nanocomposites for applications in biomedicine.

RESULTS AND DISCUSSION

Following a literature protocol,[38] we used a hydrothermal method to synthesize Fe_3O_4 nanoclusters, which were ∼50 nm clusters of ultrasmall iron oxide nanoparticles with diameters of 8−10 nm (Supporting Information Figure S1a,b,c). X-ray diffraction (XRD) data revealed that the synthesized Fe_3O_4 nanoclusters were in the cubic phase (Supporting Information Figure S2). The Fe_3O_4@PPy nanocomposites were then synthesized by an *in situ* chemical oxidative polymerization reaction occurring on the surface of Fe_3O_4 nanoclusters to obtain the core−shell nanocomposites (Figure 1a). In a typical process, $FeCl_3 \cdot 6H_2O$ was used as an oxidant to initiate the polymerization, while sodium dodecylbenzenesulfonate (SDBS) and polyvinyl alcohol (PVA, MW 9000−10 000 Da) were introduced as emulsifiers and stabilizers. To optimize the ratio between Fe_3O_4 and PPy in our nanocomposites, the reactions were performed by adding different ratios of Fe_3O_4 nanoclusters and pyrrole monomer. From the TEM images (Supporting Information Figure S1), when the ratio of Fe_3O_4 and pyrrole monomer reached 1:4, the obtained nanocomposites showed quite uniform morphology. Either the PPy shell was too thin or bare PPy nanoparticles were formed if the Fe_3O_4:pyrrole ratio was higher or lower than this optimal ratio, respectively. The introduction of SDBS and PVA was also found to be important to control the morphology of our product (Supporting Information Figure S1). We thus chose the Fe_3O_4@PPy composite synthesized under the optimized conditions (starting weight ratio of Fe_3O_4:pyrrole = 1:4) in the following experiments (Figure 1b). The actual weight ratio of Fe_3O_4:PPy in the final product was determined to be ∼1:2.5 by inductively coupled plasma (ICP) measurement of the Fe content after decomposing the nanocomposite by aqua regia.

Although as-synthesized Fe_3O_4@PPy nanoparticles were soluble in water, they would rapidly aggregate in the presence of salts and thus were not stable in physiological solutions (Supporting Information Figure S3a). To enhance the physiological stability of those nanoparticles, we then used an amphiphilic polymer, PEG-grafted poly(maleic anhydride-alt-1-octadecene) (C18PMH-PEG) (see Supporting Information for its synthesis),[39−41] to noncovalently coat Fe_3O_4@PPy nanoparticles. After PEGylation, the obtained Fe_3O_4@PPy-PEG nanoparticles were well dispersed in water, saline, and serum without any noticeable agglomeration over weeks (Supporting Information Figure S3b). The average size of Fe_3O_4@PPy observed from transmission electron microscopy (TEM) was around 100 nm (Figure 1b), while that of Fe_3O_4@PPy-PEG measured by dynamic light scattering (DLS) was around 150 nm (Supporting Information Figure S3d), indicating that those nanoparticles were mostly individually dispersed in the aqueous solution. The increased DLS measured diameter from the TEM measured diameter was likely due to the PEG coating on

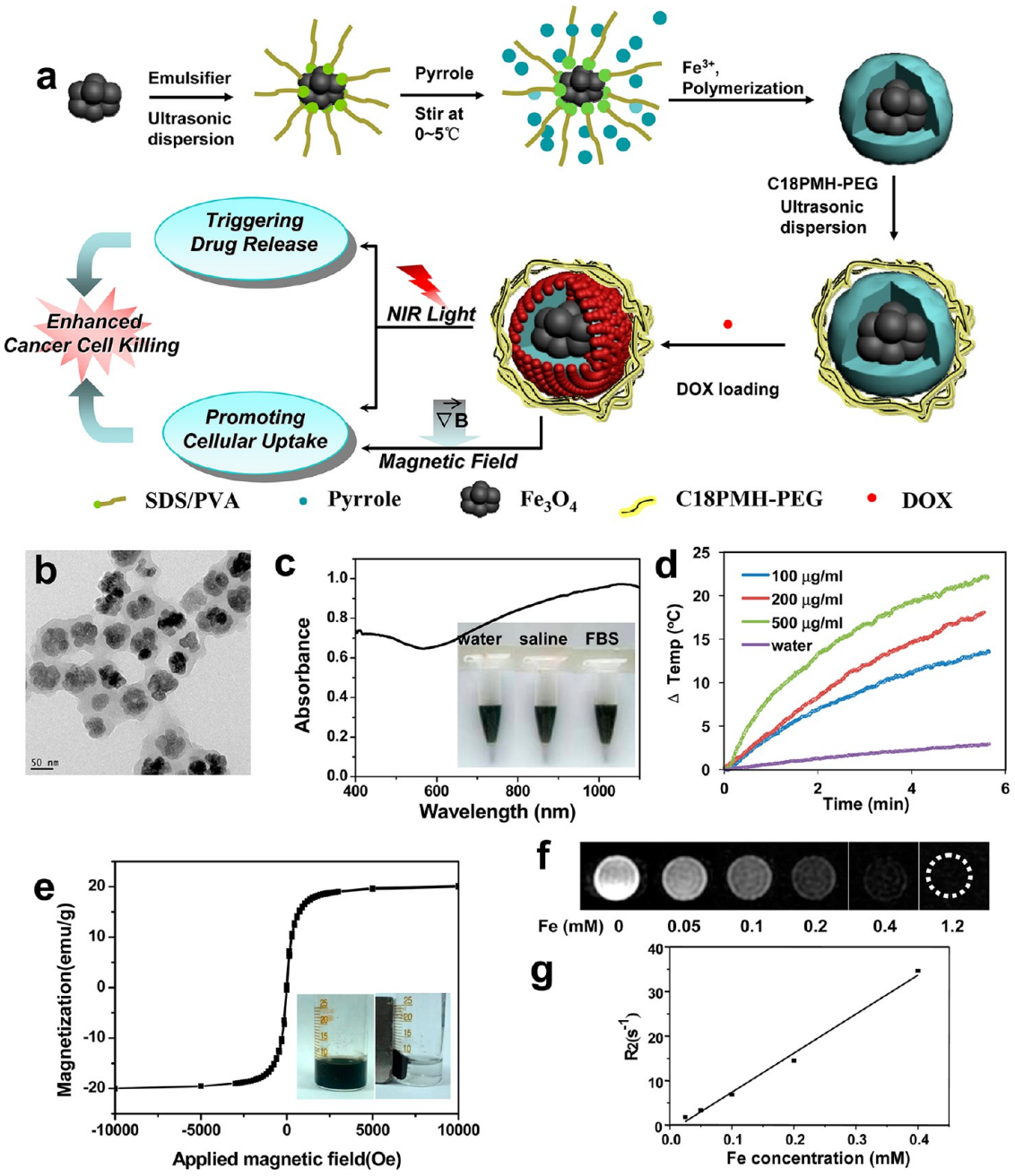

Figure 1. Preparation and characterization of Fe_3O_4@PPy-PEG nanocomposite. (a) Schematic illustration to show the synthesis of Fe_3O_4@PPy-PEG nanoparticles, the subsequent drug loading, and the remotely controlled cancer cell killing under dual physical stimuli. (b) TEM image of the synthesized Fe_3O_4@PPy-PEG nanoparticles. (c) UV−vis−NIR extinction spectra of Fe_3O_4@PPy-PEG nanoparticles in water (100 μg mL^{-1}). Inset: Photo of Fe_3O_4@PPy-PEG nanoparticles in different solutions including water, saline, and fetal bovine serum (FBS). (d) Temperature elevation of water and Fe_3O_4@PPy-PEG solution of different concentrations over a period of ~5.5 min under exposure of NIR light (808 nm, 0.75 W cm^{-2}) measured every 0.15 s using a digital thermocamera. (e) Field-dependent magnetization loop of the Fe_3O_4@PPy-PEG sample. The absence of a hystersis loop suggested the superparamagnetic property of Fe_3O_4@PPy-PEG. Inset: Photos of Fe_3O_4@PPy-PEG solutions in the absence and presence of a magnet field. (f, g) T2-weighted MR images of the nanocomposite recorded using a 3 T MR scanner revealed a concentration-dependent darkening effect, showing a high transverse relaxivity (r2) of 87 mM^{-1} s^{-1}.

the nanoparticle surface. Infrared (IR) spectra of Fe_3O_4@PPy and Fe_3O_4@PPy-PEG evidenced the polymerization of pyrrole on the surface of Fe_3O_4 and the existence of PEG in the final product, respectively (Supporting Information Figure S3c). XRD data revealed that PPy polymerization on the surface of Fe_3O_4 nanoclusters would not change their crystallinity (Supporting Information Figure S2).

The optical and magnetic properties of the obtained Fe_3O_4@PPy-PEG nanoparticles were then studied. The UV−vis−NIR absorbance spectrum showed that Fe_3O_4@PPy-PEG exhibited a high NIR absorption from 700 to 1100 nm (Figure 1c), making it a potential PTT agent. Under irradiation using an 808 nm NIR laser at a power density of 0.75 W cm^{-2}, Fe_3O_4@PPy-PEG

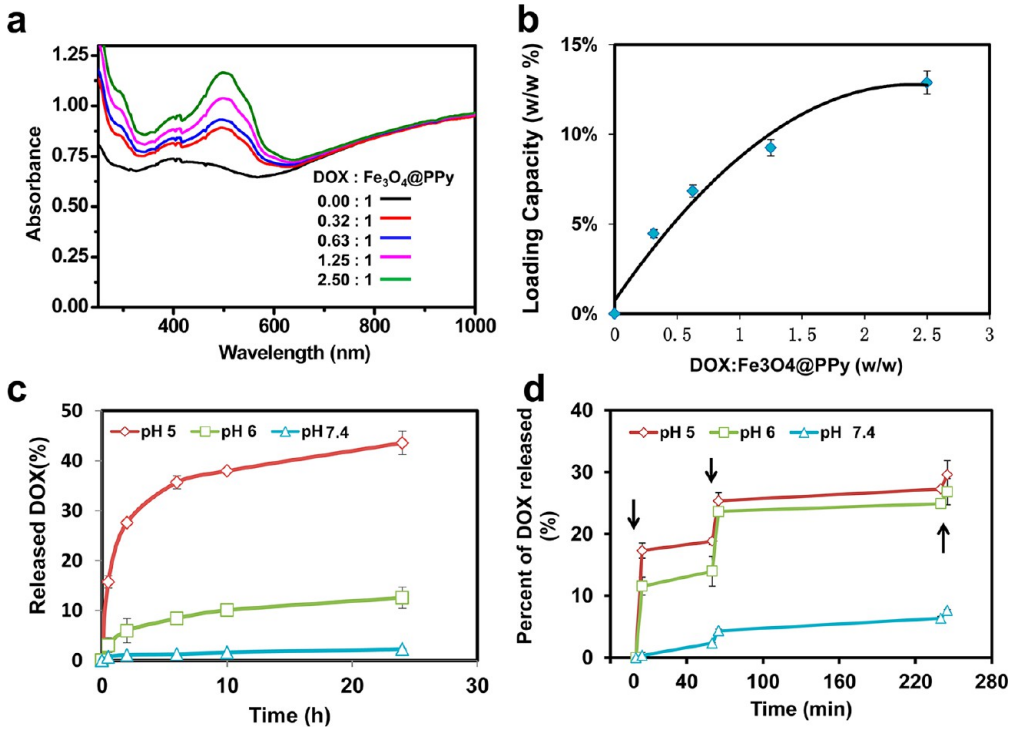

Figure 2. Drug loading and releasing. (a) UV−vis absorbance spectra of Fe_3O_4@PPy-PEG loaded with different concentrations of DOX. (b) Quantification of DOX loading at different DOX concentrations. A maximal loading of 13% by weight was obtained in our Fe_3O_4@PPy-PEG-DOX system. (c) DOX release from Fe_3O_4@PPy-PEG-DOX nanoparticles over time in buffers at the three different pH values indicated. (d) NIR-triggered release of DOX from Fe_3O_4@PPy-PEG-DOX nanoparticles. The samples at three pH values were irradiated with an NIR laser (0.75 W cm^{-2}) for 5 min at different time points indicated by the arrows. Error bars are based on at least triplicate measurements.

solutions at different concentrations showed temperature elevations of 13, 18, and 22 °C, respectively, whereas the water temperature increased by only ~3 °C under the same laser exposure (Figure 1d). Owing to the presence of a Fe_3O_4 nanocluster at the core, the Fe_3O_4@PPy-PEG nanocomposite showed strong superparamagnetism, as revealed by field-dependent magnetization measurement (Figure 1e), and thus could act as a T2 contrast agent for MR imaging (Figure 1f). T2-weighted MR images of Fe_3O_4@PPy-PEG using a 3 T MR scanner revealed a concentration-dependent darkening effect, showing a high transverse relaxivity (r2) of 87 mM^{-1} s^{-1} (Figure 1g).

It has been reported that many drug molecules with aromatic structures could be efficiently loaded on nanosurfaces with delocalized π-electrons, such as that of carbon nanotubes and graphene, *via* hydrophobic interaction and $\pi-\pi$ stacking.[42,43] We next wondered whether PPy, a conjugated hydrophobic polymer also with delocalized π-electrons, could serve as a loading and delivery platform for aromatic drugs. In our experiments, we mixed DOX, a commonly used aromatic chemotherapy drug, with Fe_3O_4@PPy-PEG in phosphate buffer (PB) solution overnight at pH 8.0. Excess unbound drug was removed by centrifugation at 14 800 rpm for 10 min, obtaining Fe_3O_4@PPy-PEG-DOX nanocomposites well dispersed in water. The UV−vis−NIR absorption spectrum of Fe_3O_4@PPy-PEG-DOX showed a DOX characteristic peak at ~490 nm, indicating the existing of DOX in the Fe_3O_4@PPy-PEG-DOX composite (Figure 2a). A significant DOX fluorescence quenching (~85%) effect was observed in the Fe_3O_4@PPy-PEG-DOX solution, suggesting the strong interaction between DOX and the nanocarrier (Supporting Information Figure S4). On the basis of a widely adapted approach to measure DOX loading on NIR-absorbing nanoparticles,[39,42,44] we used the UV−vis−NIR spectrum of Fe_3O_4@PPy-PEG-DOX to determine the DOX loading on nanoparticles, after subtracting the absorbance contribution from Fe_3O_4@PPy-PEG (normalized to be the same Fe_3O_4@PPy concentration). It was measured that the DOX loading efficiency increased with increasing amounts of added DOX, showing a saturated maximal DOX loading efficiency at ~13% (Figure 2b). It is worth noting that DOX could not be loaded on plain Fe_3O_4 nanoclusters without the PPy shell in our control experiments (data not shown), indicating no direct interaction between DOX and the Fe_3O_4 core.

Next, we used DOX-loaded Fe_3O_4@PPy-PEG-DOX nanoparticles as the model system for future studies. The drug-releasing behaviors of Fe_3O_4@PPy-PEG-DOX under different pH values were investigated by dialyzing Fe_3O_4@PPy-PEG-DOX in pH 5.0, 6.0, and 7.4 phosphate buffers (Figure 2c). The released DOX from the nanocomposite was collected and measured by fluorescence spectroscopy. Within 24 h, about 48% of DOX

was released from the nanocomposite at pH 5.0, compared with 13% and 4% of DOX release at pH 6.0 and 7.4, respectively, owing to the protonation of the amino group in the DOX molecule that offered DOX a positive charge, thus facilitating drug release under acidic pH.

We hypothesize that local heating of polymeric nanocarriers may induce increased thermal vibration of polymer chains and thus weakened binding with drug molecules. To test whether the photothermal effect of PPy can be utilized to induce DOX release from the nanocomposite, Fe_3O_4@PPy-PEG-DOX in PB solutions at pH 5.0, 6.0, and 7.4 were irradiated under an 808 nm NIR laser (0.75 W/cm^2, 5 min for each pulse). The released DOX before and after NIR laser irradiation was collected and measured, in comparison to the samples in the dark without laser irradiation (Figure 2d and Supporting Information Figure S5). The data showed that DOX release from the Fe_3O_4@PPy-PEG-DOX nanocomposite could be triggered by an external NIR laser, likely due to the loosening of PPy polymer packing resulting from a rapid local temperature increase. More interestingly, such NIR-response release processes would depend on the environmental pH. Significant NIR-triggered burst release of DOX from Fe_3O_4@PPy-PEG-DOX was noticed under acidic pH (pH = 5 or 6). In marked contrast, rather limited DOX release was observed under physiological pH (pH = 7.4) even after exposure to multiple rounds of NIR laser irradiation. This phenomenon could be useful for NIR-triggered intracellular drug release. While being stable without NIR-triggered drug release outside cells under pH 7.4, Fe_3O_4@PPy-PEG-DOX nanoparticles may release drug under NIR light exposure only after entering cell endosomes and lysosomes, where the pH value is 5−6, minimizing the unnecessary drug release before cell internalization of nanoparticles.

Before testing the remotely controlled drug delivery using our Fe_3O_4@PPy-PEG nanoplatform, we first evaluated the cytotoxicity of Fe_3O_4@PPy-PEG before and after DOX loading. Cell viability assays were carried out for 4T1 cells after various treatments. While Fe_3O_4@PPy-PEG without drug loading showed no obvious toxicity to cells even at high concentrations, Fe_3O_4@PPy-PEG-DOX rendered similar cell toxicity compared with free DOX (Supporting Information Figure S6).

We next tried several different physical parameters to stimulate the chemotherapy delivered by Fe_3O_4@PPy-PEG-DOX. The magnetic property of Fe_3O_4@PPy-PEG-DOX could be utilized for magnetically enhanced drug delivery. 4T1 cells were incubated with Fe_3O_4@PPy-PEG-DOX or free DOX at the same DOX concentration (10 μM) with or without a magnetic field for 30 min. Afterward, the cells were carefully washed to remove free nanoparticles and then reincubated for 2 h before being imaged by a confocal fluorescent microscope (Figure 3a). Cells incubated with Fe_3O_4@PPy-PEG-DOX in the presence of the magnetic field showed remarkably enhanced DOX uptake, in marked contrast to those without magnetic enhancement. Flow cytometry data revealed consistent results (Figure 3b).

In previous studies by us and others, it has been shown that a mild photothermal heating could increase the cell membrane permeability without damaging cells, enhancing the intracellular delivery of drugs or genes.[45−48] In this system, we also found that the photothermal effect of Fe_3O_4@PPy-PEG-DOX could be taken advantage of to enhance drug delivery into cancer cells. In our experiment, 4T1 cells were incubated with Fe_3O_4@PPy-PEG-DOX at 37 °C and irradiated for 10 min by an 808 nm NIR laser at a power density of 350 mW cm^{-2}. Free DOX was used as the control. After washing with phosphate-buffered saline (PBS) to fully remove excess Fe_3O_4@PPy-PEG-DOX, confocal fluorescence images were acquired (Figure 3c). It was revealed that the DOX fluorescence inside cells was significantly enhanced after laser irradiation compared to those incubated in the dark. Although the extracellular DOX release in the cell medium of pH 7.4 should be minimal based on our earlier findings (Figure 2d), we still need a better measurement approach to avoid interference from any NIR-induced drug release that could result in DOX fluorescence recovery. A quantitative DOX cell uptake assay was thus conducted by solubilizing cells by a lysis buffer, incubating cell lysates with HCl/2-propanol solvent to allow complete drug release, and measuring the DOX fluorescence in the final samples.[44,49] A nearly 2-fold increase of DOX uptake was observed after NIR laser treatment for cells incubated with Fe_3O_4@PPy-PEG-DOX, while cells incubated with the same concentration of free DOX showed no significant difference in cell uptake regardless of NIR light exposure (Figure 3d).

In order to further verify the enhanced cell uptake of nanoparticles induced by laser irradiation, we used confocal fluorescence microscopy and flow cytometry to study the cell uptake of fluorescently labeled Fe_3O_4@PPy-PEG nanoparticles without and with NIR laser irradiation (Supporting Figure S7). It was found that the cell uptake of Fe_3O_4@PPy-PEG nanoparticles, which happened under 37 °C incubation, was negligible under 4 °C incubation, indicating the cell uptake of those nanoparticles could likely be an energy-dependent endocytosis mechanism. On the other hand, the mild photothermal heating by the 808 nm laser could dramatically enhance the cell internalization of Fe_3O_4@PPy-PEG nanoparticles, consistent with our data in Figure 3c,d.

In addition to the enhanced cellular uptake of our multifunctional nanocomposite under NIR light and magnetic field, we further demonstrated that the drug release from Fe_3O_4@PPy-PEG-DOX could also be triggered by an external stimulus such as an NIR laser. In Figure 2d, we observed accelerated DOX release from Fe_3O_4@PPy-PEG-DOX under irradiation by NIR light in buffer solutions under acidic environments. Encouraged by those findings, we next studied the intracellular

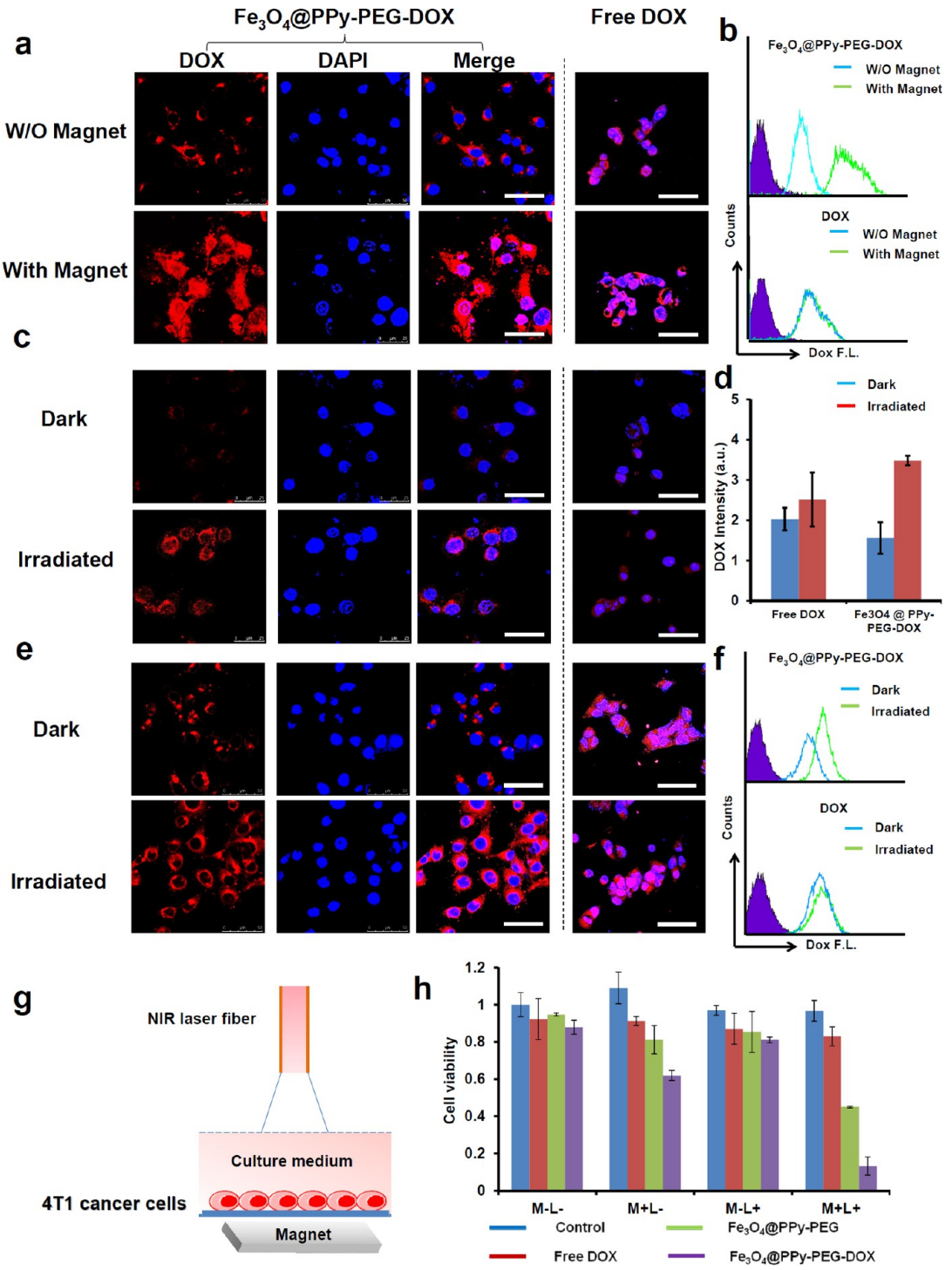

Figure 3. Drug delivery and/or release under remote optical and magnetic controls. (a) Confocal images of 4T1 cells incubated with Fe_3O_4@PPy-PEG-DOX nanoparticles (or free DOX) with or without a magnetic field for 30 min. (b) Flow cytometry measurements of cellular DOX fluorescence in (a). (c) Confocal images of 4T1 cells incubated with Fe_3O_4@PPy-PEG-DOX nanoparticles (or free DOX) with or without laser irradiation (808 nm, 350 mW cm^{-2}, 10 min). (d) Cell uptake of Fe_3O_4@PPy-DOX-PEG nanoparticles in (c) determined by the measured fluorescence intensities of cell lysate samples. (e) Confocal images showing NIR-triggered intracellular drug release. 4T1 cells preincubated with Fe_3O_4@PPy-DOX-PEG nanoparticles (or free DOX) for 2 h were washed with PBS, transferred into fresh medium, and then exposed to laser irradiation (808 nm, 350 mW cm^{-2}, 10 min). Nonirradiated samples were used as controls. (f) Flow cytometry measurements of cellular DOX fluorescence in (e). Red and blue colors in those images represent DOX fluorescence and 4′-6-diamidino-2-phenylindole (DAPI)-stained nuclear fluorescence, respectively. The scale bars are 50 μm in all confocal images. (g) Schematic illustration of *in vitro* combined therapy. (h) Relative viabilities of 4T1 cells after incubation with DOX, Fe_3O_4@PPy-PEG, and Fe_3O_4@PPy-DOX-PEG in the presence and absence of a magnetic field (30 min), with or without laser irradiation (808 nm, 350 mW cm^{-2}, 10 min). M and L represent the magnetic field and laser, respectively. The data are shown as mean ± standard deviation (SD). Error bars are based on at least triplicate measurements.

release behaviors of DOX from Fe_3O_4@PPy-PEG-DOX in response to the external NIR laser irradiation using a confocal fluorescence microscope and flow cytometry. Since the DOX fluorescence would be largely quenched in the Fe_3O_4@PPy-PEG-DOX nanocomplex (Supporting Information Figure S4), the detected DOX fluorescence recovery could be directly correlated to release of DOX inside cells (no extracellular DOX in this case). In Figure 3e, 4T1 cells were incubated with Fe_3O_4@PPy-PEG-DOX (10 μg mL^{-1}) for 2 h at 37 °C. After removal of uninternalized Fe_3O_4@PPy-PEG-DOX by extensive PBS washing, 4T1 cells were exposed to 808 nm laser irradiation at 350 mW cm^{-2} for 10 min, immediately fixed, and then imaged by confocal fluorescence microscopy. Obviously enhanced intracellular DOX fluorescence was observed in Fe_3O_4@PPy-PEG-DOX-incubated cells after laser irradiation, in comparison to those in the dark, suggesting that NIR light triggered release of DOX from internalized nanoparticles inside the cells. In the control group incubated with free DOX, no significant change was found in the cells after laser irradiation (Figure 3e). The above imaging results together with flow cytometry data (Figure 3f) evidenced that the intracellular release of DOX from Fe_3O_4@PPy-PEG-DOX could be triggered by NIR light due to the photothermally induced local heating of the nanocarrier.

We next wanted to demonstrate the enhanced cancer cell killing under both optical and magnetic external stimuli (Figure 3g). 4T1 cells were first incubated with DOX, Fe_3O_4@PPy-PEG, or Fe_3O_4@PPy-PEG-DOX for 30 min with or without a magnet placed under the cell culture plate at 37 °C. In the second step, cells were washed carefully with PBS to remove free nanoparticles and incubated for an additional 2 h. In the third step, cells were treated with or without 808 nm laser exposure at 350 mW cm^{-2} for 10 min. After further incubation for 24 h, the relative cell viabilities were determined by a standard cytotoxicity assay. As shown in Figure 3h, 4T1 cells treated with free DOX, Fe_3O_4@PPy-PEG, or Fe_3O_4@PPy-PEG-DOX without an external magnetic field showed little cytotoxicity regardless of NIR laser exposure, possibly because of the short incubation time, which gave little drug uptake by cells. Owing to the magnetically enhanced cell uptake of nanoparticles, Fe_3O_4@PPy-PEG-treated cells incubated in the presence of the magnetic field were obviously damaged after laser irradiation due to the photothermal killing (~50% of remaining cell viability). To our expectation, Fe_3O_4@PPy-PEG-DOX-incubated cells exposed to the magnetic field were also partially killed in the dark (~65% of remaining cell viability). Remarkably, cells incubated with Fe_3O_4@PPy-PEG-DOX after two types of stimuli (magnetic field + NIR laser) were nearly completely destroyed, resulting in less than 10% of remaining cell viability. These results demonstrated the enhanced cancer cell killing under both magnetic and optical external control using our multifunctional Fe_3O_4@PPy-PEG nanoparticles as the drug carrier.

Finally, we designed animal experiments to demonstrate the *in vivo* combined photothermal and chemotherapy using Fe_3O_4@PPy-PEG-DOX. Five groups of 4T1-tumor-bearing mice with five mice per group were used in our experiment. To develop the tumor model, 1×10^6 murine breast cancer 4T1 cells were subcutaneously injected into the back of each Balb/C mouse. After the tumor sizes reached about 60 mm^3 (6 days after tumor inoculation), PBS, DOX, Fe_3O_4@PPy-PEG, or Fe_3O_4@PPy-PEG-DOX solutions were administered by a single intratumoral injection (dose = 1 mg kg^{-1} DOX with 8 mg kg^{-1} Fe_3O_4@PPy-PEG). The tumors were then irradiated by the 808 nm laser at a moderate power density of 350 mW cm^{-2} for 25 min. An IR thermal camera was used to monitor the temperature changes on mice during laser irradiation (Figure 4a). Upon 808 nm laser irradiation, mice treated with Fe_3O_4@PPy-PEG or Fe_3O_4@PPy-PEG-DOX showed localized heating in the tumor region, where the temperature was maintained at 44−45 °C for 20 min. The surrounding tissue near the tumor showed only a moderate temperature increase to 35−36 °C. In contrast, the tumor temperatures of mice injected with PBS or free DOX exhibited no significant increase (below 36 °C) during 25 min of laser irradiation (Figure 4a,b).

Our earlier data (Figure 3) have evidenced that mild NIR irradiation could enhance cellular uptake of our multifunctional nanocomposite and induce intracellular drug release *in vitro*. In order to understand how mild photothermal heating would affect the *in vivo* delivery of chemotherapy, Fe_3O_4@PPy-PEG-DOX-injected tumors with or without NIR irradiation were collected 25 min after injection. After homogenizing the tumor masses, the obtained cell suspensions were washed with PBS three times and then analyzed by flow cytometry to determine the cellular DOX fluorescence. With laser irradiation (350 mW cm^{-2}, 25 min), the DOX signals of tumor cells were obviously increased compared with that of tumor cells without laser treatment (Figure 4c), indicating that NIR irradiation could enhance tumor cell uptake of our multifunctional nanoparticles and/or induce intracellular DOX release (recovery of quenched fluorescence) inside tumor cells *in vivo*. Both of these mechanisms would benefit the therapeutic outcome.

In the next two weeks, the tumor sizes and mouse body weights were measured by a caliper every other day (Figure 5a,b). Mice receiving Fe_3O_4@PPy-PEG-DOX plus NIR laser treatment showed the smallest tumor volumes, with tumor growth inhibited by ~88%. In other control groups, tumors on mice treated with DOX + laser irradiation, Fe_3O_4@PPy + laser irradiation, and Fe_3O_4@PPy-PEG-DOX without laser showed ~50%, ~30%, and ~50% growth inhibition, respectively

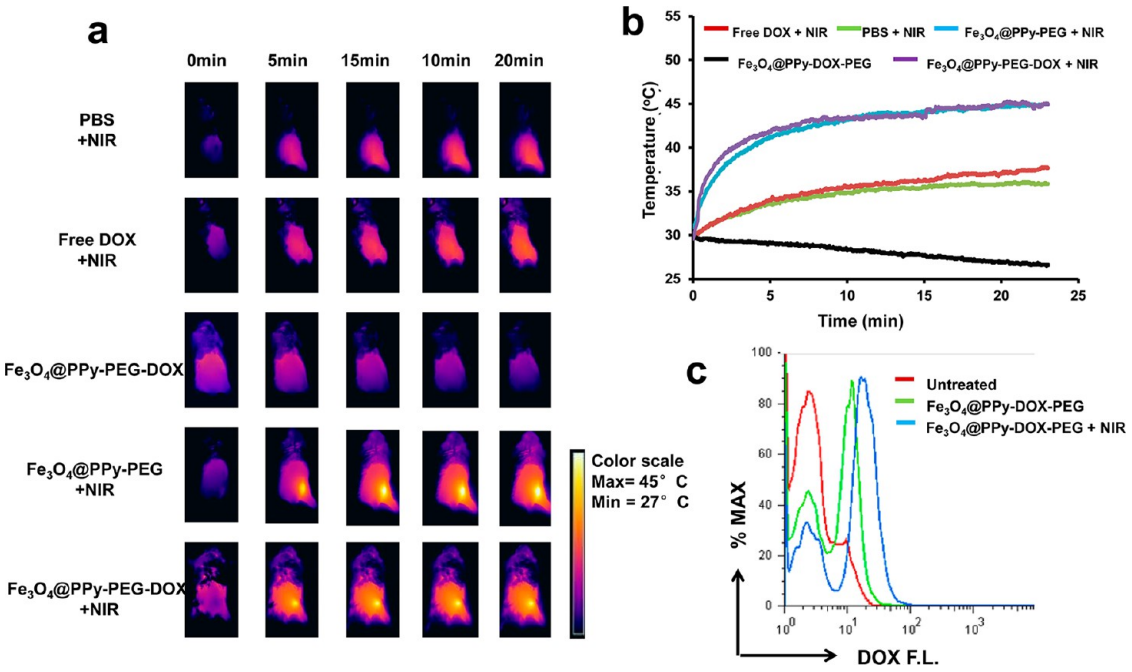

Figure 4. ***In vivo*** **photothermal tumor heating. (a) IR thermal images of tumor-bearing mice exposed (or not exposed) to the NIR laser (808 nm, 350 mW cm^{-2}, 25 min) after i.t. injection with PBS, free DOX, Fe_3O_4@PPy-PEG, or Fe_3O_4@PPy-PEG-DOX. (b) Tumor temperatures of mice monitored by the IR thermal camera during laser irradiation as indicated in (a). (c) Flow cytometry measured DOX fluorescence of tumor cells collected from Fe_3O_4@PPy-PEG-DOX-injected tumors with or without NIR laser irradiation.**

(Figure 5a,c,d). Hematoxylin and eosin (H&E) staining of tumor slices (Figure 5e) showed that while cells in untreated tumors and other control groups of tumors largely retained their normal morphology with distinctive membrane and nuclear structures, most tumor cells were severely destroyed in the group receiving both Fe_3O_4@PPy-PEG-DOX injection and NIR laser irradiation. These results are in good agreement with the tumor growth data, further confirming the superior therapeutic efficacy of the combined cancer therapy using Fe_3O_4@PPy-PEG-DOX.

The synergistic antitumor effect achieved here may be attributed to the following reasons. First of all, NIR laser irradiation of Fe_3O_4@PPy-PEG-DOX-injected tumors could enhance drug delivery into cancer cells due to mild photothermal heating, as demonstrated in our *in vitro* experiments (Figure 3c,d). Second, after cell internalization, exposure to the NIR laser would induce the release of DOX from Fe_3O_4@PPy-PEG-DOX inside cells (Figure 3e,f), enhancing chemotherapeutic efficacy. Third, cancer cells treated with local hyperthermia for 20 min at 44 °C under NIR laser treatment could be more susceptible to the damage caused by chemotherapy, as illustrated in previous studies.[50,51] At last, the heat shock caused by laser irradiation around 44 °C may involve direct cell killing as the result of protein denaturing and aggregation, or indirect killing due to the triggering of programmed cell death mechanisms such as apoptosis by the proteotoxic stress.[52−54]

Although in our subcutaneous tumor model the tumor sizes could be measured simply by a caliper, advanced imaging techniques, such as magnetic resonance imaging, have to be used for monitoring primary tumor models in animals and real clinical evaluations of tumors in patients. Since superparamagnetic Fe_3O_4 nanoparticles are well known as excellent contrast agents in T2-weighted MR imaging (Figure 1f,g), our Fe_3O_4@PPy-PEG-DOX nanocomposite thus could serve as a theranostic agent for imaging-guided cancer therapy. In our experiment, MR images were obtained at day 0 (before and after injection) and day 7 (after injection). The acquired T2-weighted MR images showed that after injection with Fe_3O_4@PPy-PEG-DOX a rather strong darkening effect in the tumor area was observed (Figure 5f). Continuous monitoring by MR imaging provided tumor development information after combined therapy, consistent with the results obtained by the caliper measurement, demonstrating the possibility of using our multifunctional Fe_3O_4@PPy-PEG-DOX nanocomposite for imaging-guided cancer therapy.

Toxic side effects have been a major drawback in chemotherapy treatment of cancer. In our experiments, it was observed that the body weights of mice were not significantly affected after receiving various different treatments, except for those treated with free DOX, which resulted in a significant body weight loss (10%) in the first two days (Figure 5b). Histology analysis of major organs from mice 14 days after Fe_3O_4@PPy-PEG-DOX injection and laser treatment indicated no appreciable abnormality or noticeable organ damage (Supporting Information Figure S10), suggesting the PPy-containing nanocomposites developed here were not obviously toxic

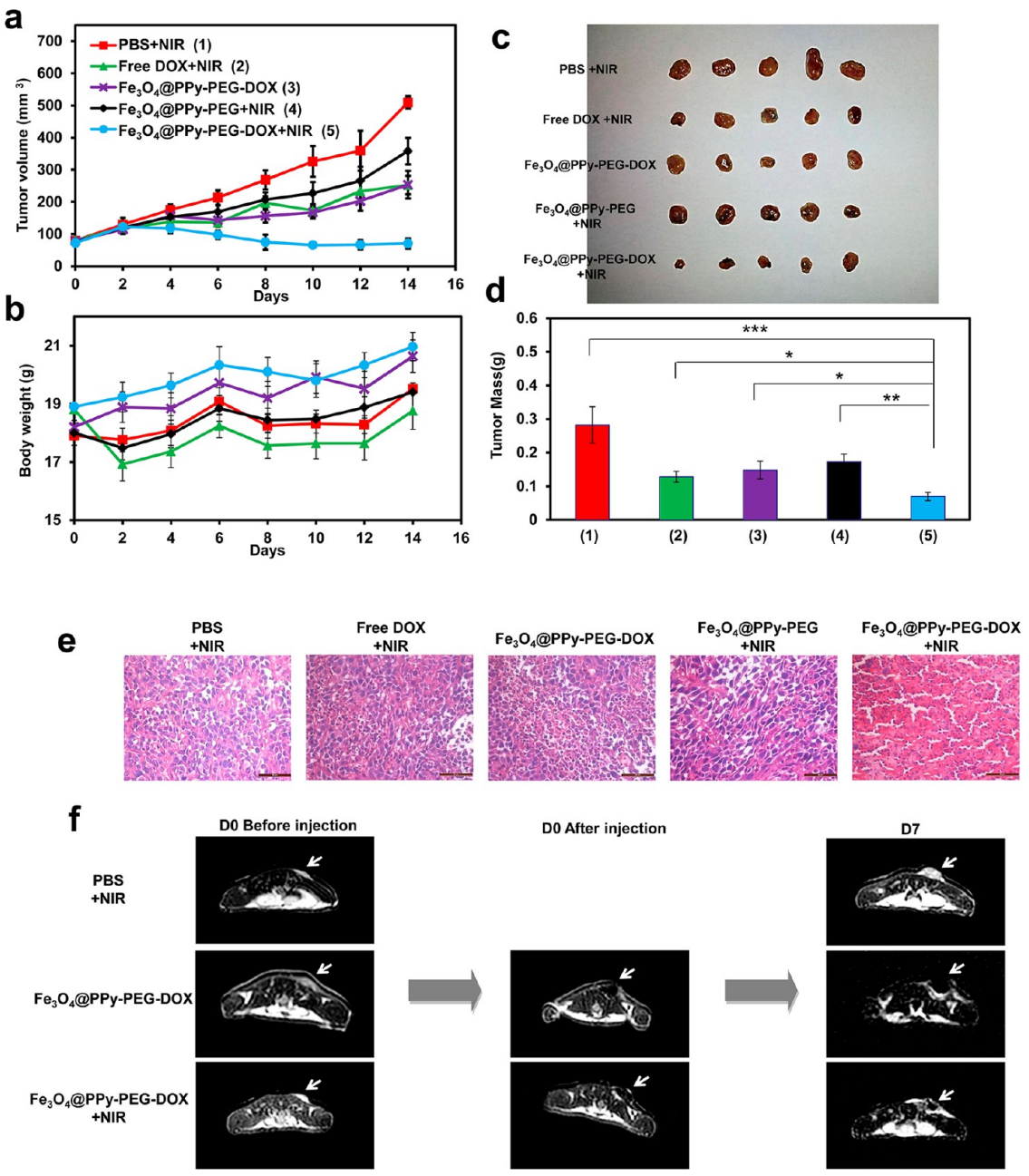

Figure 5. ***In vivo*** **combination cancer therapy. (a) Tumor growth curves of different groups of mice after various treatments indicated (5 mice per group). Error bars are based on standard errors of the mean (SEM). (b) Body weights of mice after various treatments indicated. (c) Photos of the tumors collected from different groups of mice at the end of treatments (day 14). (d) Average weights of tumors collected from mice at the end of various treatments indicated. Error bars are based on SEM (*** $p < 0.001$, ** $p < 0.01$, or * $p < 0.05$, by ANOVA with Tukey's post-test) (e) H&E-stained tumor slices collected from mice post various treatments indicated (scale bar = 50 μm). (f) Representative MR images of mice from three different groups obtained at day 0 before and after injection and day 7 after treatment (tumors marked by the white arrow).**

after local administration into mice at the current dose. However, further studies should be planned to carefully look into the dose-dependent toxicology of PPy and PPy-based nanocomposites to treated animals after systemic administration.

To further improve the efficacy of our combination therapy based on Fe_3O_4@PPy-PEG-DOX, we then tried a higher power density during NIR laser irradiation. PBS, Fe_3O_4@PPy-PEG, or Fe_3O_4@PPy-PEG-DOX solutions (the same dose as mentioned previously) were administered by a single intratumoral injection into 4T1-tumor-bearing mice. By increasing the laser power density to ~425 mW cm^{-2}, we were able to control the final temperature of Fe_3O_4@PPy-PEG-injected tumor to be between 48 and 49 °C (Figure 6a,b). As expected, tumors injected with PBS exhibited no significant temperature increase (~37 °C) during 25 min of laser irradiation (Figure 6a,b). The tumor sizes and body weights after various treatments were then monitored. While the tumor growth could be greatly inhibited by

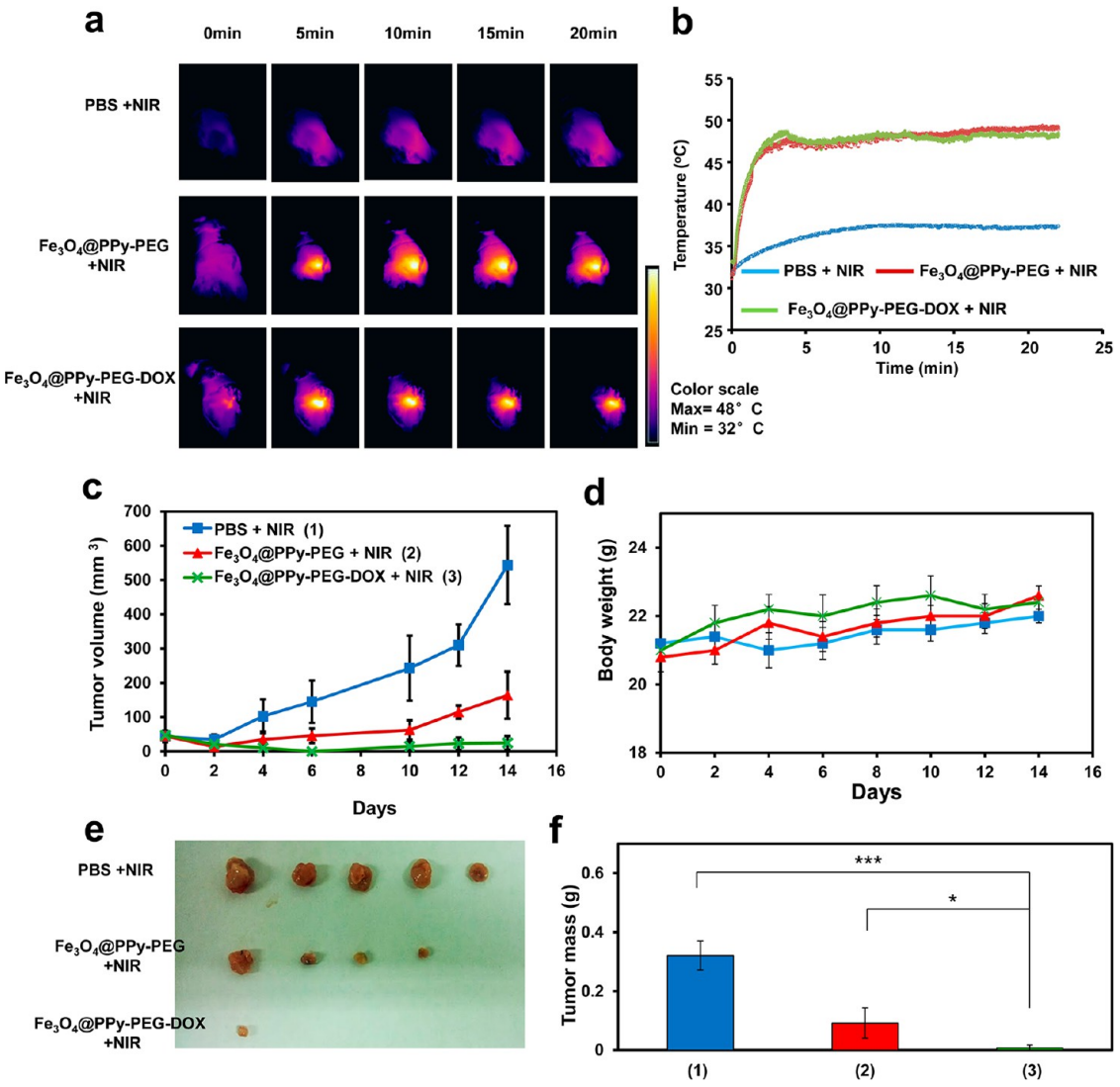

Figure 6. Cancer combination therapy with increased laser power density. (a) IR thermal images of tumor-bearing mice exposed to the NIR laser (808 nm, 425 mW cm^{-2}, 25 min) after i.t. injection with PBS, Fe_3O_4@PPy-PEG, or Fe_3O_4@PPy-PEG-DOX. (b) Tumor temperatures of mice monitored by the IR thermal camera during laser irradiation as indicated in (a). (c) Tumor growth curves of different groups of mice after various treatments indicated (5 mice per group). Error bars are based on SEM. (d) Body weights of mice after various treatments indicated. (e) Photos of the tumors collected from different groups of mice at the end of treatments (day 14). (f) Average weights of tumors collected from mice at the end of various treatments indicated. Error bars are based on SEM (*$p < 0.001$, **$p < 0.01$, or *$p < 0.05$, by ANOVA with Tukey's post-test). Note that in the combination treatment group, 4 out of 5 tumors were completely eliminated after treatment.**

just the photothermal effect of Fe_3O_4@PPy-PEG without DOX loading, the combination of photothermal therapy and chemotherapy offered by Fe_3O_4@PPy-PEG-DOX under laser irradiation was even more effective and resulted in complete eradication of most tumors (4 out of 5) (Figure 6c–f). Therefore, in future application of photothermal and chemo- combined therapy, the photothermal effect induced by a high power laser irradiation could directly kill tumor cells by heating and at least eliminate part of the tumor. On the other hand, if on certain occasions it is not realistic to homogeneously deliver sufficient light power into the whole tumor mass (*e.g.*, when the tumors are big), the synergic therapeutic effect offered by the combination therapy could still be remarkable in inhibiting the tumor development.

CONCLUSIONS

In conclusion, a novel type of theranostic agent based on Fe_3O_4@PPy core–shell structured nanoparticles is synthesized by *in situ* polymerization and then coated with PEG for improved water solubility and biocompatibility. In this multifunctional nanocomposite, the iron oxide nanocluster core, which should be biodegradable and nontoxic, is utilized to magnetically control drug delivery, as well as to serve as the contrast agent in T2-weighted MR imaging. The PPy, which is a polymer widely used for tissue engineering applications,[24,26–28] also offers a number of different functionalities. Owing to its hydrophobic structure with delocalized π-electrons, PPy could bind with aromatic drug molecules such as DOX, for drug loading and delivery. On the other hand,

PPy, with strong NIR absorption, exhibits a strong photothermal effect, which is useful to kill cancer cells directly by hyperthermia or indirectly by promoting cross-membrane drug delivery and triggering intracellular drug release to enhance chemotherapeutic efficiency. Utilizing the above interesting properties of our Fe_3O_4@PPy-PEG nanocomposite, highly effective combined photothermal and chemotherapy is demonstrated in our *in vivo* cancer treatment study, whose therapeutic outcome can be recorded by MR imaging. Because this system also works for the loading of other aromatic therapeutic molecules (*e.g.*, photodynamic agents Chlorin e6 and Indocyanine green, Supporting Information Figure S10), it is expected that the further combination of photothermal therapy with chemotherapy, photodynamic therapy, and even magnetic hypothermia may offer great opportunities in the development of new cancer therapeutic approaches. Further studies are ongoing in our laboratory to realize cancer combination therapy using these multifunctional nanoparticles upon systemic administration. Overall, our study presents a novel multifunctional theranostic agent useful in imaging-guided, remotely controlled cancer therapy with excellent synergistic antitumor effect and promises further development of NIR-absorbing organic nanoparticles and organic−inorganic nanocomposites for phototherapy and combined therapy of cancer.

MATERIALS AND METHODS

Materials. Ferric chloride hexahydrate ($FeCl_3 \cdot 6H_2O$), sodium acetate (CH_3COONa, NaOAc), ethylene glycol (EG), diethylene glycol (DEG), and poly(vinylpyrrolidone) (PVP, K30) were purchased from Sinopharm Chemical Reagent Co., Ltd. Pyrrole, dodecylbenzenesulfonic acid sodium salt (SDBS), and polyvinyl alcohol (PVA, MW 9000−10 000) were purchased from Sigma-Aldrich. Doxorubicin (DOX) was bought from Beijing HuaFeng United Technology Co. Ltd. All chemicals were of analytical grade and used without further purification.

Synthesis of Fe_3O_4 Nanoclusters. Fe_3O_4 nanoclusters were synthesized using a literature method with slight modifications. $FeCl_3 \cdot 6H_2O$ (2 mmol) was dissolved in a mixture of EG and DEG (V_{EG}/V_{DEG} = 4:16, total volume was 20 mL) in a beaker under magnetic stirring. After 30 min, 2 g of PVP was added to the above solution and the suspension was heated at 120 °C to give a transparent solution. After an hour, 1.5 g of NaOAc was added into the above solution while heating was stopped. After vigorous stirring for a further 30 min, the obtained homogeneous solution was transferred into a Teflon-lined stainless-steel autoclave (25 mL volume), which was sealed and then heated at 200 °C. After a 12 h reaction period, the autoclave was cooled to room temperature. The obtained ferrite nanoclusters were washed three times with ethanol and water and then dried under vacuum for 12 h.

Preparation of Fe_3O_4@PPy-PEG. The Fe_3O_4@PPy composites were synthesized by an *in situ* chemical oxidative polymerization in the presence of Fe_3O_4 nanoclusters. $FeCl_3 \cdot 6H_2O$ was used as an oxidant to initiate the polymerization, while SDBS and PVA were introduced as emulsifiers and stabilizers. In a typical procedure, 5 mg of Fe_3O_4 nanoclusters was added into an aqueous solution containing 5 mg of SDBS and 15 mg of PVA. The solution was then ultrasonicated for over 30 min to make Fe_3O_4 well dispersed. The solution was then stirred at room temperature for 2 h before 20 μL of pyrrole monomer was added into the mixture. After further stirring for 30 min, 20 mg of $FeCl_3$ was dropwisely added into the reaction mixture. Finally, the mixture was polymerized for 12 h at room temperature to obtain Fe_3O_4@PPy core−shell nanocomposites with a dark green color. The resulting nanoparticles were washed with deionized water three times and then separated by a magnet to remove excess PPy and other reagents. To estimate the Fe_3O_4:PPy weight ratio in the nanocomposite, the Fe_3O_4 content was determined by the ICP measured Fe concentration, and the total weight of the composite was measured by weighing the completely dried form of the final Fe_3O_4@PPy product.

C18PMH-PEG was synthesized following our previously established protocol. In brief, 10 mg of poly(maleic anhydride-alt-1-octadecene) (C18PMH) and 143 mg of mPEG-NH_2 (5 K) were dissolved in 5 mL of dichloromethane, and 6 μL of triethylamine (TEA) and 11 mg of 1-ethyl-3-(3-dimethylaminopropyl)carbodiimide (EDC) were added. After 24 h of reaction, the solvent was evaporated and the solid product was dissolved in water. After removal of excess reagents by dialysis, the final product, C18PMH-PEG (44.9% of carboxyl groups in C18PMH were PEGylated as determined by NMR), was freeze-dried and stored at −20 °C before use.

C18PMH-PEG-NH_2 was synthesized following our previously established protocol. In brief, 10 mg (1 equiv) of C18PMH, 143 mg (1 equiv) of mPEG-NH_2(5k), and 50 mg (0.5 equiv) of NH_2-mPEG(5k)-BOC (Polymere, Germany) were mixed together in dichloromethane under agitation to form a homogeneous solution. EDC (2 equiv) and TEA (8 equiv) were then added under magnetic stirring. After stirring for 24 h at room temperature, the dichloromethane solvent was blown-dried by nitrogen. Subsequently, 2 mL of trifluoroacetic acid (TFA, Sinopharm Chemical Reagent Co.) was added under magnetic stirring for 3 h at room temperature to deprotect the Boc group. After evaporating the TFA solvent, the leftover solid was dissolved in water and dialyzed for 2 days in a dialysis bag (MWCO = 14 kDa) to remove unreacted PEG polymers and other reagents. After lyophilization, the final product (C18PMH-PEG-NH_2) as a white solid was stored at −20 °C for future use. To conjugate fluorescein to C18PMH-PEG-NH_2, 100 mg of C18PMH-PEG-NH_2 was mixed with 5 mg of NHS-fluorescein (Pierce). After 24 h of reaction at room temperature, the yielded C18PMH-PEG-FITC was purified by dialysis against water using a 14 kDa membrane and then freeze-dried.

To prepare Fe_3O_4@PPy-PEG (or Fe_3O_4@PPy-PEG-FITC), Fe_3O_4@PPy was dispersed in water to obtain a clear solution. A solution of C18PMH-PEG (or Fe_3O_4@PPy-PEG-FITC) at 2 mg/mL was added into the Fe_3O_4@PPy solution, which was ultrasonicated for 30 min. The final product was purified by centrifugation several times.

Drug Loading and Release of Fe_3O_4@PPy-PEG-DOX Nanocomplex. In a typical experiment, loading of DOX onto Fe_3O_4@PPy-PEG nanocomposite was accomplished by mixing a DOX hydrochloride solution in water (10 mg/mL) at the desired volume with a Fe_3O_4@PPy-PEG solution (1 mg/mL) in phosphate buffer (PB, 2 mM, pH 8.0). The mixture was placed in the oscillation shaker in the dark overnight. Excess DOX was removed by centrifugation and washing with PB several times. The obtained Fe_3O_4@PPy-PEG-DOX nanocomplex was stored at 4 °C in the dark for future use. The loading of Ce6 and ICG on Fe_3O_4@PPy-PEG was conducted following the same procedure used for DOX loading, except that the loading pH was 7.4 instead of 8.0.

The release of DOX from Fe_3O_4@PPy-PEG-DOX was studied by dialyzing the sample under 37 °C in PB (2 mM) at pH 5.0, 6.0, and 7.4 for different periods of time. DOX released from nanocomposites was collected and determined by its fluorescence spectrum.

The laser-triggered drug release experiments were performed in PB (2 mM) at pH 5.0, 6.0, and 7.4 at 37 °C. An optical-fiber-coupled power-tunable diode laser (continuous wave) with wavelengths of 808 nm (maximal power = 10 W) was employed in this work. Fe_3O_4@PPy-PEG-DOX was dispersed in 5 mL of PB solution at different pH's. At desired time intervals,

the samples were irradiated by the 808 nm laser with a power intensity of 0.75 W/cm^2 for 5 min. As the controls, Fe_3O_4@PPy-PEG-DOX solutions without laser irradiation were used. For each measurement, 500 μL of solution was centrifuged at 10 000 rpm for 5 min. The amount of released DOX in the supernatant was determined using UV−vis spectrometry.

Characterization. Transmission electron microscopy images were taken using a Philips CM300 transmission electron microscope operating at an acceleration voltage of 200 kV. The phase and crystallography of the product was characterization by using a Shimadzu XRD-6000 X-ray diffractometer equipped with Cu Kα radiation (λ = 0.154 06 nm). Fluorescence spectra were obtained on a FluoroMax 4 spectrometer (Horiba Jobin Yvon). UV−vis−NIR spectra were acquired by using a PerkinElmer Lambda 750 UV/vis spectrophotometer. Laser irradiation was performed using an optical-fiber-coupled power-tunable diode laser (continuous wave) (maximal power = 10 W, Hi-Tech Optoelectronics Co., Beijing, China).

Cellular Experiments. The 4T1 murine breast cancer cell line was originally obtained from American Type Culture Collection (ATCC) and cultured under recommended conditions. The *in vitro* cytotoxicity was measured using a standard methyl thiazolyltetrazolium (MTT, Sigma Aldrich) assay or a CytoTox 96 nonradioactive cytotoxicity assay (Promega). For the MTT assay, 4T1 cells were seeded into 96-well cell culture plates at 1 $\times$ 10^5/well until adherent and then incubated with various concentrations of Fe_3O_4@PPy-PEG-DOX, Fe_3O_4@PPy-PEG, and free DOX for 24 h. The standard MTT assay was carried out to determine the cell viabilities relative to the control untreated cells. For the CytoTox assay, 4T1 cells were seeded into 96-well plates at 1 $\times$ 10^5/well until adherent and then incubated with Fe_3O_4@PPy-PEG-DOX, Fe_3O_4@PPy-PEG, and free DOX with or without a magnetic field for ~0.5 h. Afterward, cells were washed twice with PBS and incubated in fresh cell medium for an additional 2 h. Then the cells were irradiated by an 808 nm laser (350 mW cm^{-2}) for 10 min. The cell viabilities were determined with the CytoTox96 nonradioactive cytotoxicity assay (Promega, G1780) following the vendor's protocol.

Confocal fluorescence images of cells were taken by a Lecia SP5 laser scanning confocal microscope. For flow cytometry measurement, cells after trypsin treatment were washed with PBS twice and then analyzed using a Calibur flow cytometer (BD Biosciences, USA).

Animal Experiments. Female Balb/c mice were purchased from Nanjing Peng Sheng Biological Technology Co. Ltd. and used under protocols approved by Soochow University Laboratory Animal Center. 4T1 cells (1 $\times$ 10^6) suspended in 40 μL of PBS were subcutaneously injected into the back of each female Balb/c mouse. After ~6 days, the mice bearing 4T1 tumors were treated when the tumor volume reached ~60 mm^3. The mice were divided into five groups (n = 5 per group) and intratumorally injected with 20 μL of PBS, DOX, Fe_3O_4@PPy-PEG, and Fe_3O_4@PPy-PEG-DOX (DOX 1 mg/kg, Fe_3O_4@PPy 8 mg/kg). After injection, tumors were irradiated with or without NIR light (350 mW cm^{-2}, 808 nm) for 25 min. Tumor sizes were monitored every 2 days for 2 weeks. The length and width of the tumors were measured by a digital caliper. The tumor volume was calculated according to the following formula: width^2 $\times$ length/2.

For flow cytometry measurement, mice with tumors injected with Fe_3O_4@PPy-PEG-DOX, with or without NIR laser irradiation (350 mW cm^{-2}, 808 nm, 25 min), were sacrificed by CO_2 inhalation. Tumors were removed using forceps and surgical scissors and then homogenized. After filtration through a 70 μm nylon filter, tumor cell suspensions were washed three times with complete RPMI-1640 medium and analyzed using a Calibur flow cytometer (BD Biosciences, USA) for DOX fluorescence measurement. FACS data were analyzed using Flowjo.

IR Thermal Imaging. Mice bearing 4T1 tumors treated with PBS, Fe_3O_4@PPy-PEG, or Fe_3O_4@PPy-PEG-DOX were irradiated with the 808 nm laser at power densities of 350 mW/cm^{-2} for 25 min and simultaneously imaged by an IR thermal camera (Infrared Cameras. Inc.).

MR Imaging. Fe_3O_4@PPy-PEG-DOX samples were scanned under a 3 T clinical MRI scanner (Bruker Biospin Corporation, Billerica, MA, USA) at room temperature. After acquiring the T2-weighted MR images, the T2 intensities of images were measured within manually drawn regions of interest for each sample. Relaxation rates R2 (R2 = 1/T2) were calculated from T2 values at different iron concentrations. MR imaging of mice was accomplished with the same 3 T clinical MR scanner equipped with a special coil used for small-animal imaging.

Histology and Immunohistochemistry. Two weeks after various treatments, animals were sacrificed with tumors and other major organs collected for analysis. The tissue sections were stained with H&E following the standard protocol. All sections were examined under a Leica microscope.

Conflict of Interest: The authors declare no competing financial interest.

Supporting Information Available: More detailed materials characterization data (TEM images, XRD data, IR data, DLS data fluorescence spectra, *etc.*), drug release data, cell toxicity data, fluorescence microscope data, photos of mice after various treatments, images of H&E-stained tissue slices, and loading data of two other types of therapeutic molecules are available free of charge *via* the Internet at http://pubs.acs.org.

Acknowledgment. This work was partially supported by the National Basic Research Programs of China (973 Program) (2012CB932600, 2011CB911002), the National Natural Science Foundation of China (51222203, 51132006, 51002100), and a Project Funded by the Priority Academic Program Development (PAPD) of Jiangsu Higher Education Institutions.

REFERENCES AND NOTES

1. Huebsch, N.; Mooney, D. J. Inspiration and Application in the Evolution of Biomaterials. *Nature* **2009**, *462*, 426–432.
2. Davis, M. E.; Chen, Z.; Shin, D. M. Nanoparticle Therapeutics: an Emerging Treatment Modality for Cancer. *Nat. Rev. Drug Discovery* **2008**, *7*, 771–782.
3. Troutman, T. S.; Leung, S. J.; Romanowski, M. Light-Induced Content Release from Plasmon-Resonant Liposomes. *Adv. Mater.* **2009**, *21*, 2334–2338.
4. Yang, X.; Liu, X.; Liu, Z.; Pu, F.; Ren, J.; Qu, X. Near-Infrared Light-Triggered, Targeted Drug Delivery to Cancer Cells by Aptamer Gated Nanovehicles. *Adv. Mater.* **2012**, *24*, 2890–2895.
5. Jayakumar, M. K. G.; Idris, N. M.; Zhang, Y. Remote Activation of Biomolecules in Deep Tissues Using Near-Infrared-to-UV Upconversion Nanotransducers. *Proc. Natl. Acad. Sci. U.S.A.* **2012**, *109*, 8483–8488.
6. Baeza, A.; Guisasola, E.; Ruiz-Hernández, E.; Vallet-Regí, M. Magnetically Triggered Multidrug Release by Hybrid Mesoporous Silica Nanoparticles. *Chem. Mater.* **2012**, *24*, 517–524.
7. Ge, J.; Neofytou, E.; Cahill, T. J.; Beygui, R. E.; Zare, R. N. Drug Release from Electric-Field-Responsive Nanoparticles. *ACS Nano* **2012**, *6*, 227–233.
8. Thomas, C. R.; Ferris, D. P.; Lee, J.-H.; Choi, E.; Cho, M. H.; Kim, E. S.; Stoddart, J. F.; Shin, J.-S.; Cheon, J.; Zink, J. I. Noninvasive Remote-Controlled Release of Drug Molecules *in Vitro* Using Magnetic Actuation of Mechanized Nanoparticles. *J. Am. Chem. Soc.* **2010**, *132*, 10623–10625.
9. Schroeder, A.; Honen, R.; Turjeman, K.; Gabizon, A.; Kost, J.; Barenholz, Y. Ultrasound Triggered Release of Cisplatin from Liposomes in Murine Tumors. *J. Controlled Release* **2009**, *137*, 63–68.
10. Melancon, M. P.; Zhou, M.; Li, C. Cancer Theranostics with Near-Infrared Light-Activatable Multimodal Nanoparticles. *Acc. Chem. Res.* **2011**, *44*, 947–956.
11. Yang, K.; Zhang, S.; Zhang, G.; Sun, X.; Lee, S. T.; Liu, Z. Graphene in Mice: Ultrahigh *in Vivo* Tumor Uptake and Efficient Photothermal Therapy. *Nano Lett.* **2010**, *10*, 3318–3323.
12. Liu, X.; Tao, H.; Yang, K.; Zhang, S.; Lee, S. T.; Liu, Z. Optimization of Surface Chemistry on Single-Walled Carbon Nanotubes for *in Vivo* Photothermal Ablation of Tumors. *Biomaterials* **2011**, *32*, 144–151.
13. Xiao, Z. Y.; Ji, C. W.; Shi, J. J.; Pridgen, E. M.; Frieder, J.; Wu, J.; Farokhzad, O. C. DNA Self-Assembly of Targeted Near-Infrared-Responsive Gold Nanoparticles for Cancer Thermo-Chemotherapy. *Angew. Chem., Int. Ed.* **2012**, *51*, 11853–11857.

14. Kang, H.; Trondoli, A. C.; Zhu, G.; Chen, Y.; Chang, Y. J.; Liu, H.; Huang, Y. F.; Zhang, X.; Tan, W. Near-Infrared Light-Responsive Core-Shell Nanogels for Targeted Drug Delivery. *ACS Nano* **2011**, *5*, 5094–5099.
15. Ma, Y.; Liang, X.; Tong, S.; Bao, G.; Ren, Q.; Dai, Z. Gold Nanoshell Nanomicelles for Potential Magnetic Resonance Imaging, Light-Triggered Drug Release, and Photothermal Therapy. *Adv. Funct. Mater.* **2013**, *23*, 815–822.
16. Zhang, Z.; Wang, L.; Wang, J.; Jiang, X.; Li, X.; Hu, Z.; Ji, Y.; Wu, X.; Chen, C. Mesoporous Silica-Coated Gold Nanorods as a Light-Mediated Multifunctional Theranostic Platform for Cancer Treatment. *Adv. Mater.* **2012**, *24*, 1418–1423.
17. Chen, J.; Glaus, C.; Laforest, R.; Zhang, Q.; Yang, M.; Gidding, M.; Welch, M. J.; Xia, Y. Gold Nanocages as Photothermal Transducers for Cancer Treatment. *Small* **2010**, *6*, 811–817.
18. Chen, J.; Yang, M.; Zhang, Q.; Cho, E. C.; Cobley, C. M.; Kim, C.; Glaus, C.; Wang, L. V.; Welch, M. J.; Xia, Y. Gold Nanocages: A Novel Class of Multifunctional Nanomaterials for Theranostic Applications. *Adv. Funct. Mater.* **2010**, *20*, 3684–3694.
19. Yang, K.; Wan, J.; Zhang, S.; Tian, B.; Zhang, Y.; Liu, Z. The Influence of Surface Chemistry and Size of Nanoscale Graphene Oxide on Photothermal Therapy of Cancer Using Ultra-Low Laser Power. *Biomaterials* **2012**, *33*, 2206–2214.
20. Huang, X.; Tang, S.; Mu, X.; Dai, Y.; Chen, G.; Zhou, Z.; Ruan, F.; Yang, Z.; Zheng, N. Freestanding Palladium Nanosheets with Plasmonic and Catalytic Properties. *Nat. Nanotechnol.* **2011**, *6*, 28–32.
21. Tian, Q.; Tang, M.; Sun, Y.; Zou, R.; Chen, Z.; Zhu, M.; Yang, S.; Wang, J.; Wang, J.; Hu, J. Hydrophilic Flower-Like CuS Superstructures as an Efficient 980 nm Laser-Driven Photothermal Agent for Ablation of Cancer Cells. *Adv. Mater.* **2011**, *23*, 3542–3547.
22. Cheng, L.; Yang, K.; Chen, Q.; Liu, Z. Organic Stealth Nanoparticles for Highly Effective *in Vivo* Near-Infrared Photothermal Therapy of Cancer. *ACS Nano* **2012**, *6*, 5605–5613.
23. Peer, D.; Karp, J. M.; Hong, S.; Farokhzad, O. C.; Margalit, R.; Langer, R. Nanocarriers as an Emerging Platform for Cancer Therapy. *Nat. Nanotechnol.* **2007**, *2*, 751–760.
24. Yang, K.; Xu, H.; Cheng, L.; Sun, C.; Wang, J.; Liu, Z. *In Vitro* and *in Vivo* Near-Infrared Photothermal Therapy of Cancer Using Polypyrrole Organic Nanoparticles. *Adv. Mater.* **2012**, *24*, 5586–5592.
25. Yang, J.; Choi, J.; Bang, D.; Kim, E.; Lim, E.-K.; Park, H.; Suh, J.-S.; Lee, K.; Yoo, K.-H.; Kim, E.-K.; *et al*. Convertible Organic Nanoparticles for Near-Infrared Photothermal Ablation of Cancer Cells. *Angew. Chem., Int. Ed.* **2011**, *50*, 441–444.
26. Oh, W. K.; Yoon, H.; Jang, J. Size Control of Magnetic Carbon Nanoparticles for Drug Delivery. *Biomaterials* **2010**, *31*, 1342–1348.
27. George, P. M.; Lyckman, A. W.; LaVan, D. A.; Hegde, A.; Leung, Y.; Avasare, R.; Testa, C.; Alexander, P. M.; Langer, R.; Sur, M. Fabrication and Biocompatibility of Polypyrrole Implants Suitable for Neural Prosthetics. *Biomaterials* **2005**, *26*, 3511–3519.
28. Fonner, J. M.; Forciniti, L.; Nguyen, H.; Byrne, J. D.; Kou, Y. F.; Syeda-Nawaz, J.; Schmidt, C. E. Biocompatibility Implications of Polypyrrole Synthesis Techniques. *Biomed. Mater.* **2008**, *3*, 034124.
29. Ramanaviciene, A.; Kausaite, A.; Tautkus, S.; Ramanavicius, A. Biocompatibility of Polypyrrole Particles: An *in-Vivo* Study in Mice. *J. Pharm. Pharmacol.* **2007**, *59*, 311–315.
30. Wang, X. D.; Gu, X. S.; Yuan, C. W.; Chen, S. J.; Zhang, P. Y.; Zhang, T. Y.; Yao, J.; Chen, F.; Chen, G. Evaluation of Biocompatibility of Polypyrrole *in Vitro* and *in Vivo*. *J. Biomed. Mater. Res. Part A* **2004**, *68*, 411–422.
31. Abidian, M. R.; Corey, J. M.; Kipke, D. R.; Martin, D. C. Conducting-Polymer Nanotubes Improve Electrical Properties, Mechanical Adhesion, Neural Attachment, and Neurite Outgrowth of Neural Electrodes. *Small* **2010**, *6*, 421–429.
32. Yoon, H.; Lee, S. H.; Kwon, O. S.; Song, H. S.; Oh, E. H.; Park, T. H.; Jang, J. Polypyrrole Nanotubes Conjugated with Human Olfactory Receptors: High-Performance Transducers for FET-Type Bioelectronic Noses. *Angew. Chem., Int. Ed.* **2009**, *48*, 2755–2758.
33. Kwon, O. S.; Park, S. J.; Jang, J. A High-Performance VEGF Aptamer Functionalized Polypyrrole Nanotube Biosensor. *Biomaterials* **2010**, *31*, 4740–4747.
34. Runge, M. B.; Dadsetan, M.; Baltrusaitis, J.; Ruesink, T.; Lu, L. C.; Windebank, A. J.; Yaszemski, M. J. Development of Electrically Conductive Oligo(polyethylene glycol) Fumarate-Polypyrrole Hydrogels for Nerve Regeneration. *Biomacromolecules* **2010**, *11*, 2845–2853.
35. Runge, M. B.; Dadsetan, M.; Baltrusaitis, J.; Knight, A. M.; Ruesink, T.; Lazcano, E. A.; Lu, L.; Windebank, A. J.; Yaszemski, M. J. The Development of Electrically Conductive Polycaprolactone Fumarate-Polypyrrole Composite Materials for Nerve Regeneration. *Biomaterials* **2010**, *31*, 5916–5926.
36. Chen, M.; Fang, X.; Tang, S.; Zheng, N. Polypyrrole Nanoparticles for High-Performance *in Vivo* Near-Infrared Photothermal Cancer Therapy. *Chem. Commun. (Cambridge, U.K.)* **2012**, *48*, 8934–8936.
37. Zha, Z.; Yue, X.; Ren, Q.; Dai, Z. Uniform Polypyrrole Nanoparticles with High Photothermal Conversion Efficiency for Photothermal Ablation of Cancer Cells. *Adv. Mater.* **2013**, *25*, 777–782.
38. Xuan, S. H.; Wang, F.; Wang, Y. X. J.; Yu, J. C.; Leung, K. C. F. Facile Synthesis of Size-Controllable Monodispersed Ferrite Nanospheres. *J. Mater. Chem.* **2010**, *20*, 5086–5094.
39. Wang, C.; Cheng, L.; Liu, Z. Drug Delivery with Upconversion Nanoparticles for Multi-functional Targeted Cancer Cell Imaging and Therapy. *Biomaterials* **2011**, *32*, 1110–1120.
40. Wang, C.; Ma, X. X.; Ye, S. Q.; Cheng, L.; Yang, K.; Guo, L.; Li, C. H.; Li, Y. G.; Liu, Z. Protamine Functionalized Single-Walled Carbon Nanotubes for Stem Cell Labeling and *in Vivo* Raman/Magnetic Resonance/Photoacoustic Triple-Modal Imaging. *Adv. Funct. Mater.* **2012**, *22*, 2363–2375.
41. Wang, C.; Cheng, L.; Xu, H.; Liu, Z. Towards Whole-Body Imaging at the Single Cell Level Using Ultra-sensitive Stem Cell Labeling with Oligo-arginine Modified Upconversion Nanoparticles. *Biomaterials* **2012**, *33*, 4872–4881.
42. Liu, Z.; Sun, X. M.; Nakayama-Ratchford, N.; Dai, H. J. Supramolecular Chemistry on Water-Soluble Carbon Nanotubes for Drug Loading and Delivery. *ACS Nano* **2007**, *1*, 50–56.
43. Liu, Z.; Robinson, J. T.; Sun, X. M.; Dai, H. J. PEGylated Nanographene Oxide for Delivery of Water-Insoluble Cancer Drugs. *J. Am. Chem. Soc.* **2008**, *130*, 10876–10877.
44. Liu, Z.; Fan, A. C.; Rakhra, K.; Sherlock, S.; Goodwin, A.; Chen, X. Y.; Yang, Q. W.; Felsher, D. W.; Dai, H. J. Supramolecular Stacking of Doxorubicin on Carbon Nanotubes for *in Vivo* Cancer Therapy. *Angew. Chem., Int. Ed.* **2009**, *48*, 7668–7672.
45. Tian, B.; Wang, C.; Zhang, S.; Feng, L. Z.; Liu, Z. Photothermally Enhanced Photodynamic Therapy Delivered by Nano-Graphene Oxide. *ACS Nano* **2011**, *5*, 7000–7009.
46. Feng, L.; Yang, X.; Shi, X.; Tan, X.; Peng, R.; Wang, J.; Liu, Z. Polyethylene Glycol and Polyethylenimine Dual-Functionalized Nano-Graphene Oxide for Photothermally Enhanced Gene Delivery. *Small* **2013**, 10.1002/smll.201202538.
47. Sherlock, S. P.; Tabakman, S. M.; Xie, L. M.; Dai, H. J. Photothermally Enhanced Drug Delivery by Ultrasmall Multifunctional FeCo/Graphitic Shell Nanocrystals. *ACS Nano* **2011**, *5*, 1505–1512.
48. Sherlock, S. P.; Dai, H. J. Multifunctional FeCo-graphitic Carbon Nanocrystals for Combined Imaging, Drug Delivery and Tumor-Specific Photothermal Therapy in Mice. *Nano Res.* **2011**, *4*, 1248–1260.
49. Laginha, K. M.; Verwoert, S.; Charrois, G. J. R.; Allen, T. M. Determination of Doxorubicin Levels in Whole Tumor and Tumor Nuclei in Murine Breast Cancer Tumors. *Clin. Cancer. Res.* **2005**, *11*, 6944–6949.
50. Atkinson, R. L.; Zhang, M.; Diagaradjane, P.; Peddibhotla, S.; Contreras, A.; Hilsenbeck, S. G.; Woodward, W. A.; Krishnan, S.; Chang, J. C.; Rosen, J. M. Thermal Enhancement with Optically Activated Gold Nanoshells Sensitizes Breast Cancer Stem Cells to Radiation Therapy. *Sci. Transl. Med.* **2010**, *2*, 55ra79–55ra79.

51. Pelicci, P. G.; Dalton, P.; Orecchia, R. Heating Cancer Stem Cells to Reduce Tumor Relapse. *Breast Cancer Res.* **2011**, *13*, 305–307.
52. Core, D. M. *Hyperthermia and Cancer*; Plenum Press: New York, 1982.
53. Gabai, V. L.; Meriin, A. B.; Yaglom, J. A.; Volloch, V. Z.; Sherman, M. Y. Role of Hsp70 in Regulation of Stress-Kinase JNK: Implications in Apoptosis and Aging. *FEBS Lett.* **1998**, *438*, 1–4.
54. Mukhopadhaya, A.; Mendecki, J.; Dong, X. Y.; Liu, L. B.; Kalnicki, S.; Garg, M.; Alfieri, A.; Guha, C. Localized Hyperthermia Combined with Intratumoral Dendritic Cells Induces Systemic Antitumor Immunity. *Cancer Res.* **2007**, *67*, 7798–7806.